The Canadian Mineralogist
Vol. 36, pp. 215-227 (1998)

COMPOSITIONAL CONTROLS ON PHASE-TRANSITION TEMPERATURES IN BORNITE: A DIFFERENTIAL SCANNING CALORIMETRY STUDY

BENJAMIN A. GRGURIC[1]

Department of Earth Sciences, University of Cambridge, Downing Street, Cambridge CB2 3EQ, U.K.

ANDREW PUTNIS

Institut für Mineralogie, Universität Münster, Corrensstrasse 24, D-48149 Münster, Germany

Abstract

Structural phase transitions in bornite (Cu_5FeS_4) are associated with distinctive thermal anomalies. We investigated variations in the phase-transition temperatures of bornite using differential scanning calorimetry (DSC). The composition of 48 samples of natural and synthetic low bornite was determined using an electron microprobe operating in WDS mode. Temperatures of the low–intermediate and intermediate–high transitions of these samples were then determined by performing heating and cooling DSC scans over the range 50–300°C. Heating-run peaks of thermal anomalies associated with the low–intermediate transition varied over the ranges 197–207°C in natural samples and 154–201°C in synthetic samples of bornite. The thermal anomalies associated with the intermediate–high transition occur between 259 and 273°C in natural samples, and between 239 and 271°C in synthetic bornite. The marked variations in temperatures of the intermediate–high transition are linearly related to the Fe content and the Cu:Fe ratio. No such relationships are associated with the low–intermediate transition, implying the existence of fundamental differences in the mechanisms of the two transitions. On average, synthetic samples of bornite underwent the low–intermediate transition at lower temperatures than natural samples, this phenomenon being attributed to the possible presence of a larger population of quenched-in vacancies and the lower concentration of trace impurities in synthetic bornite.

Keywords: bornite, differential scanning calorimetry, copper iron sulfide, Cu_5FeS_4, phase transitions.

Sommaire

Les deux inversions structurales de la bornite (Cu_5FeS_4) se manifestent par des anomalies thermiques distinctes. Nous avons étudié les variations dans la température de ces inversions en utilisant la calorimétrie différentielle à balayage. Nous avons établi la composition chimique de 48 échantillons de bornite naturelle et synthétique avec une microsonde électronique en dispersion de longueurs d'onde. La température des transitions entre bornite de basse température et bornite intermédiaire d'une part, et bornite intermédiaire et bornite de haute température de l'autre, a ensuite été déterminée en balayant les transitions en chauffant et en refroidissant les échantillons sur l'intervalle 50–300°C. L'anomalie thermique associée à la première transition, telle qu'obtenue en réchauffant, a lieu entre 197 et 207°C dans la bornite naturelle, et entre 154 et 201°C dans la bornite synthétique. L'anomalie thermique due à la transition entre bornite intermédiaire et bornite de haute température a lieu entre 259 et 273°C dans les échantillons naturels, et entre 239 et 271°C dans la bornite synthétique. Les grandes variations en température de cette dernière transition dépendent de façon linéaire de la teneur en Fe et du rapport Cu:Fe. Aucune conclusion semblable ne semble expliquer la première transition, à plus faible température, ce qui impliquerait l'existence de différences fondamentales dans le mécanisme des deux inversions. En moyenne, la bornite synthétique se transforme de la forme basse température à la forme intermédiaire à température plus faible que les échantillons naturels, phénomène attribuable à la présence possible d'une population plus élevée de lacunes et à une plus faible concentration d'impuretés à l'état de traces dans les échantillons synthétiques.

(Traduit par la Rédaction)

Mots-clés: bornite, calorimétrie différentielle par balayage, sulfure de cuivre et de fer, Cu_5FeS_4, inversions structurales.

[1] *E-mail address*: bag21@esc.cam.ac.uk

INTRODUCTION

Bornite (Cu_5FeS_4) is an important copper ore mineral of widespread occurrence in diverse geological settings, from deep-level mafic intrusions to the supergene enrichment zones of ore deposits, formed at near-ambient conditions. Commonly associated with other phases in the system Cu–Fe–S, it forms a complete solid-solution with digenite ($Cu_{8.9}Fe_{0.1}S_5$) and a limited solid-solution with chalcopyrite ($CuFeS_2$) at elevated temperatures. Bornite occurs in three temperature-dependent polymorphs related by a simple scheme of superstructures (Koto & Morimoto 1975, Putnis & Grace 1976, Pierce & Buseck 1978). The relationships among these three polymorphs have been the subject of several crystallographic studies since the recognition of a temperature-dependent phase transition in bornite by Frueh (1950). Initially considered to result from fine-scale twinning (Morimoto & Kullerud 1961), this mechanism for polymorphism was later shown to be inconsistent with transmission electron microscopy (TEM) observations and superstructuring proposed in its place (Putnis & Grace 1976). The actual mechanisms of the phase transitions associated with polymorphism in bornite have never been entirely resolved owing to the difficulty of distinguishing Cu atoms from Fe using X-ray techniques, which has hindered precise structural refinements of the polymorphs. A clearer understanding of the mechanisms and energetics of these phase transitions is of importance in the thermodynamic treatment of ore assemblages, especially since the transitions in question occur within the typical temperature range of hydrothermal processes responsible for ore deposition.

CRYSTAL STRUCTURE, POLYMORPHISM AND CHEMISTRY

The basic structural unit of bornite is that of a zinc–blende-type, face-centered cubic sulfur lattice with Cu and Fe atoms located in tetrahedral interstices. In stoichiometric bornite 25% of these tetrahedral sites are vacant, giving the true formula $Cu_5Fe\square_2S_4$. The cubic (*Fm*3*m*) structure of high bornite, stable above approximately 270°C, consists of a fundamental sulfur cell (a = 5.47 Å) with a disordered distribution of vacant tetrahedra, and Cu and Fe atoms statistically distributed over 24 equivalent sites in each occupied tetrahedron (Kanazawa *et al.* 1978). This phase is unquenchable. Between approximately 270° and 200°C the intermediate bornite structure is stable (Kanazawa *et al.* 1978, Grguric *et al.* 1996). This structure is also cubic *Fm*3*m*, and the transition from the high form involves a doubling of the high bornite cell, giving a 2a superstructure. The mechanism proposed for this transition involves a long-range cation-ordering and vacancy-clustering process, resulting in a structure consisting of alternating Fe-containing and Fe-free a subcells (Kanazawa *et al.* 1978). This structure can be quenched, but slowly inverts to low bornite at room temperature (Morimoto & Kullerud 1961). Low bornite, stable below approximately 190°C, is orthorhombic (*Pbca*) with a 2a4a2a superstructure. Off-centering of metal atoms in tetrahedral sites (Koto & Morimoto 1975) and short-range vacancy-ordering (Pierce & Buseck 1978) are proposed mechanisms for the intermediate–low transition. Natural stoichiometric bornite is always of the orthorhombic low form; certain samples of S-rich bornite from low-temperature supergene and red-bed-type Cu-deposits, however, lack some of the characteristic powder-diffraction lines of stoichiometric bornite (Yund & Kullerud 1966), and so may possess a different superstructure. Despite the ease of synthesis for compositions across the whole bornite–digenite join, all of which share an identical fundamental substructure, and the large degree of solid-solution behavior at elevated temperatures, bornite from natural occurrences exhibits compositional variation that is invariably limited to within a few atomic % of stoichiometry. Natural samples of digenite exhibit a similar lack of compositional variation; it is significant that there are no known occurrences of intermediate members of the extensive bornite–digenite solid solution in nature. The degree of compositional variation in bornite and its influence on phase transitions are the focus of this study.

PHASE-TRANSITION TEMPERATURES

The early single-crystal X-ray investigations of bornite polymorphism by Morimoto & Kullerud (1961) and Morimoto (1964) relied on sample heating and quenching routines rather than *in situ* measurements to determine phase-transition temperatures, and their results have since been shown to be incorrect by later investigators using calorimetric and *in situ* high-temperature diffraction methods (Kanazawa *et al.* 1978, Robie *et al.* 1994, Grguric *et al.* 1996). Their method of study also led to the erroneous conclusion that the structure of intermediate bornite is not stable over a discrete range of temperature but is only produced by rapid quenching from above 228°C. All three polymorphs and associated transitions were observed in the TEM studies of Putnis & Grace (1976) and Pierce & Buseck (1978), but since the electron beam itself was used to induce temperature changes in the sample, temperature measurements were not possible. Differential scanning calorimetry (DSC) is an ideal method for the study of the thermal anomalies associated with phase transitions in bornite owing to its high precision of temperature measurement (±0.25°C), the low temperatures of the transitions in question, and their relatively large enthalpies, which result in excellent peak-to-baseline contrast. DSC analysis of bornite has previously been described by Kanazawa *et al.* (1978) and Robie *et al.* (1994). In their work on the heat capacity of bornite, Robie *et al.* (1994) noted

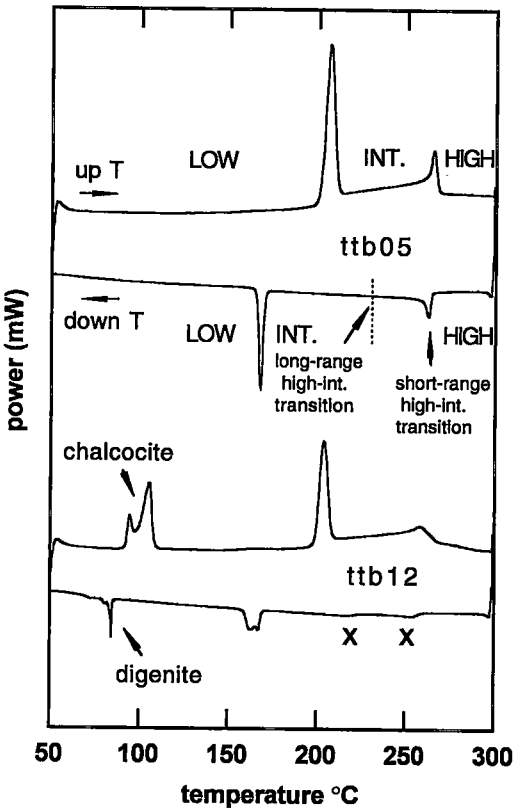

FIG. 1. DSC scan profiles of natural bornite (top) and chalcocite-contaminated natural bornite (bottom). Heating and cooling scan rates are 10° and 5°C/minute, respectively. Down-T re-appearance of the long-range 2*a* cubic superstructure is shown by the stippled line (Grguric *et al.* 1998). In the contaminated sample, the doublet of the chalcocite α–β transition in the heating scan is replaced by the single high–low transition peak of digenite during the cooling scan. "X" indicates high–intermediate transitions in bornite. See text for explanation.

discrepancies between the transition temperatures determined in their study and those quoted by earlier investigators, in particular Pankratz & King (1970) and Kanazawa *et al.* (1978), all of whom used synthetic material, with one natural sample considered in the latter study. Transition temperatures quoted in these different studies varied between 187 and 212°C and between 257 and 267°C for the low–intermediate and intermediate–high transitions, respectively. Robie *et al.* ascribed these differences to small compositional variations among samples used in the various studies, differences in temperature calibration of the instrument, and in the case of Pankratz & King, to errors associated with the determination of exact temperatures of transitions using drop calorimetry. Our basis for a more detailed investigation of the possible controls on transition temperatures was the initial observation of a 21°C difference between the peaks of the thermal anomalies associated with the low–intermediate transition of a synthetic bornite and that of a sample from the Magma mine, Arizona, in preliminary DSC scans. Since both samples were analyzed on the same instrument under identical conditions, we tentatively concluded that minor compositional variations are responsible for this difference. This study was initiated with the aim of investigating and quantifying the effects of this variation on the transition temperatures in bornite utilizing a group of natural and synthetic samples, with the overall aim of providing possible insight into the mechanisms responsible for each transition. Our previous work on phase transitions in natural bornite (Grguric *et al.* 1998) showed that the thermal anomalies measured using DSC correspond to structural transitions associated with polymorphism (observed using *in situ* neutron powder diffraction) in heating scans. The situation was complicated in cooling runs by kinetic effects associated with the growth of antiphase domains, which displaces the development of the long-range 2*a* superstructure some 30° below the temperature of the short-range high–intermediate transition peak recorded by DSC (Fig. 1).

SAMPLE PREPARATION

Small (4–8 mm) chips of natural bornite from several locations (Table 1) were extracted from ore samples and trimmed of other sulfides and adhering gangue. Each chip was hand-ground into a flat plate approximately 0.5–0.8 mm thick and 3–4 mm across for DSC analysis. This sample geometry greatly assists heat transfer and temperature equilibration between the sample and the heat source of the calorimeter. Sample masses were in the range 35–40 mg. Following DSC analysis, the chips were mounted in cold-set epoxy resin for polishing, optical examination, and electron-microprobe analysis.

Synthetic bornite was produced by heating weighed quantities of high-purity (99.999%) elemental Cu, Fe and S in vacuum-sealed silica-glass capsules. A length of silica-glass rod and silica wool were also included in each capsule to minimize the amount of vacuum space and to insulate the charge during sealing. After initial reaction at 950°C for 5 days, the capsules were slowly cooled over 24 hours, broken open, and the charges finely ground, with the entire grinding process being carried out under acetone to inhibit oxidation. These charges were then resealed in silica-glass capsules and heated at 950°C for a further 14 days to homogenize the sulfide. The capsules were then cooled to room temperature over 24 hours. Samples richer in S than 40 atomic % were cooled to 650°C over 24 hours, and then quenched in water. Quenching hinders the

TABLE 1. BORNITE SAMPLES SELECTED, AND COMPOSITIONAL DATA

Sample	Location	Deposit Type†	Cu wt.%	Fe wt.%	S wt.%	Total wt.%	Cu at.%	Fe at.%	S at.%	Me:S atomic	Cu:S atomic	Fe:S atomic	Cu:Fe atomic	Contam. phases††
ttb01	4600' Level, Magma Mine, Arizona	m	63.38	10.96	25.55	99.88	50.11	9.86	40.03	1.498	1.252	0.246	5.083	
ttb02	4600' Level, Magma Mine, Arizona	m	62.89	11.32	25.72	99.93	49.62	10.16	40.22	1.487	1.234	0.253	4.882	
ttb03	Magma Mine, Arizona	m	63.28	11.34	25.54	100.15	49.91	10.17	39.92	1.505	1.250	0.255	4.907	
ttb04	390R.L., Olympic Dam Mine, Sth. Australia	m	63.66	11.08	25.26	100.00	50.39	9.98	39.63	1.523	1.272	0.252	5.050	
ttb05	420R.L., Olympic Dam Mine, Sth. Australia	m	62.83	11.34	25.76	99.93	49.55	10.18	40.27	1.483	1.231	0.253	4.870	
ttb06	410R.L., Olympic Dam Mine, Sth. Australia	m	63.31	11.25	25.48	100.04	50.00	10.11	39.89	1.507	1.254	0.254	4.945	cc
ttb07	410R.L., Olympic Dam Mine, Sth. Australia	m	63.50	11.08	25.42	100.00	50.21	9.97	39.83	1.511	1.260	0.250	5.038	
ttb08	Moonta Mines, Moonta, South Australia	h/m	63.56	10.99	25.47	100.02	50.23	9.88	39.90	1.507	1.259	0.248	5.086	
ttb09	Gortdrum Mine, County Tipperary, Ireland	m	63.45	11.11	25.50	100.06	50.11	9.98	39.91	1.506	1.255	0.250	5.019	
ttb10	Whitehorse Mine, Yukon Territory, Canada	s	63.77	10.67	25.41	99.85	50.51	9.61	39.88	1.507	1.266	0.241	5.256	
ttb11	Mt. Gunson Mine, South Australia	d	63.66	10.70	25.65	100.00	50.26	9.61	40.13	1.492	1.252	0.239	5.230	cc
ttb12	Mt. Gunson Mine, South Australia	d	64.37	10.49	25.08	99.93	51.08	9.47	39.44	1.535	1.295	0.240	5.393	cc
ttb13	Junction Mine, Bisbee, Arizona	m	63.43	10.96	25.62	100.01	50.08	9.85	40.08	1.495	1.249	0.246	5.085	
ttb14	Kombat Mine, near Grootfontein, Namibia	m	63.53	10.98	25.52	100.02	50.18	9.86	39.95	1.503	1.256	0.247	5.088	
ttb15	Mt. Gunson Mine, South Australia	d	63.68	11.03	25.28	99.99	50.41	9.93	39.66	1.522	1.271	0.250	5.076	cc
ttb16	Kupferschiefer, Eisleben, Germany	d	63.72	10.98	25.33	100.04	50.40	9.88	39.72	1.518	1.269	0.249	5.099	
ttb17	Kupferschiefer, Sangerhausen, Germany	d	64.23	10.48	25.24	99.96	50.89	9.45	39.64	1.522	1.284	0.238	5.387	
ttb18	Stewart vein, 3600' Level, Butte, Montana	m	64.61	10.52	24.92	100.05	51.29	9.50	39.21	1.550	1.308	0.242	5.400	dj
ttb19	Stewart vein, 3600' Level, Butte, Montana	m	64.03	10.90	25.10	100.04	50.74	9.83	39.43	1.536	1.287	0.249	5.163	
ttb20	Kipushi Mine, Shaba Province, Zaire	m	64.12	10.80	25.04	99.95	50.88	9.75	39.37	1.540	1.292	0.248	5.221	
ttb21	Mufulira Mine, Copperbelt, Zambia	ms	63.91	10.86	25.25	100.02	50.60	9.78	39.63	1.524	1.277	0.247	5.174	m.cc
ttb22	Run 069a	syn	64.45	10.77	24.80	100.03	51.21	9.74	39.05	1.561	1.311	0.249	5.259	
ttb23	Run 069b	syn	63.82	11.09	25.05	99.95	50.62	10.00	39.38	1.540	1.286	0.254	5.060	
ttb24	Run 070a	syn	63.90	10.91	25.22	100.02	50.60	9.83	39.57	1.527	1.279	0.248	5.149	
ttb25	Run 070b	syn	64.19	10.57	25.25	100.03	50.82	9.52	39.63	1.523	1.283	0.240	5.337	
ttb26	Run 071a	syn	65.61	9.96	24.49	100.05	52.29	9.03	38.68	1.585	1.352	0.233	5.792	mix
ttb27	Run 071b	syn	64.71	10.81	24.44	99.97	51.58	9.81	38.62	1.590	1.336	0.254	5.260	mix
ttb28	Run 072a	syn	65.27	9.86	24.91	100.05	51.86	8.92	39.22	1.550	1.322	0.227	5.817	tr.dg
ttb29	Run 072b	syn	65.12	10.03	24.90	100.04	51.73	9.06	39.21	1.551	1.319	0.231	5.709	tr.dg
ttb30	Run 073a	syn	63.60	11.36	24.98	99.95	50.46	10.26	39.28	1.546	1.285	0.261	4.919	mix
ttb31	Run 073b	syn	63.47	11.52	25.01	100.00	50.31	10.39	39.30	1.545	1.280	0.264	4.842	mix
ttb32	Run 074a	syn	64.29	10.56	25.18	100.02	50.94	9.52	39.54	1.529	1.289	0.241	5.352	
ttb33	Run 074b	syn	64.54	10.37	25.13	100.05	51.16	9.35	39.48	1.533	1.296	0.237	5.470	
ttb34	Run 075a	syn	64.62	10.48	24.83	99.92	51.39	9.48	39.13	1.556	1.313	0.242	5.421	
ttb35	Run 075b	syn	64.32	10.68	25.00	100.00	51.04	9.65	39.32	1.543	1.298	0.245	5.291	
ttb36	Run 076a	syn	62.63	11.87	25.49	99.99	49.45	10.66	39.89	1.507	1.240	0.267	4.638	
ttb37	Run 076b	syn	62.86	11.56	25.56	99.98	49.62	10.38	40.00	1.500	1.241	0.260	4.780	
ttb38	Run 077a	syn	64.15	11.23	24.66	100.04	50.99	10.16	38.85	1.574	1.313	0.262	5.019	mix
ttb39	Run 077b	syn	63.20	11.66	25.17	100.03	50.03	10.50	39.48	1.533	1.267	0.266	4.766	mix
ttb40	Run 3-10-96 (a)	syn	63.85	10.92	25.21	99.97	50.58	9.84	39.58	1.527	1.278	0.249	5.140	
ttb41	Run 3-10-96 (b)	syn	63.75	11.08	25.11	99.95	50.55	10.00	39.45	1.535	1.281	0.253	5.056	
ttb42	Run 3-10-96 (c)	syn	64.49	10.74	24.75	99.98	51.28	9.72	39.00	1.564	1.315	0.249	5.279	
ttb43	Run 005	syn	63.97	10.94	24.84	99.75	50.92	9.91	39.17	1.553	1.300	0.253	5.138	dg
ttb44	Run 052 doped with 1000ppm Ag	syn	63.44	11.16	25.25	99.84	50.28	10.06	39.66	1.521	1.268	0.254	4.998	
ttb45	Run 053 doped with 900ppm Se	syn	64.24	10.86	24.88	99.98	51.03	9.81	39.16	1.554	1.303	0.251	5.200	
ttb46	Run 054 doped with 850ppm Bi	syn	63.99	10.74	24.94	99.67	50.94	9.73	39.34	1.542	1.295	0.247	5.236	
ttb47	Run 055 doped with 800ppm As	syn	63.93	10.94	24.87	99.75	50.87	9.91	39.22	1.550	1.297	0.253	5.135	
ttb48	Run 075b	syn	64.09	10.66	25.19	99.94	50.81	9.61	39.58	1.526	1.284	0.243	5.287	tr.dg

† m= mesothermal; h/m= hypo/mesothermal; s= skarn; d= diagenetic; ms= metasedimentary; syn= dry synthetic

†† cc= chalcocite; dj= djurleite; m.cc= minor chalcocite; mix= complex mixture; tr.dg= trace digenite; dg= digenite

exsolution of digenite or chalcopyrite or both in these nonstoichiometric samples, as can occur during slow cooling or annealing below 650°C (Brett & Yund 1964, Yund & Kullerud 1966). Inversion from the initially formed metastable *2a*-superstructured cubic polymorph to low bornite (*2a4a2a*-orthorhombic) occurs at room temperature within a few days of quenching from synthesis temperatures (Morimoto & Kullerud 1961); slow cooling, as performed here on the stoichiometric and S-deficient samples, however, allows the transformation to low bornite to occur within the cooling period, as verified by our previous *in situ* neutron diffraction experiments (Grguric *et al.* 1998). Polished mounts of the synthetic samples were examined using a reflected-light microscope, and found to consist of polycrystalline intergrowths, with individual grain-sizes on the order of 0.5–2 mm. The samples of synthetic bornite were prepared as flat plates for microprobe and DSC analysis as described above.

Thermal Analysis

The basic principle of differential scanning calorimetry involves subjecting a sample and an identical reference-container (empty in this case) to a linear temperature program and measuring the heat-flow rate into the sample. A primary temperature-control system monitors the average temperature of the two containers, while a secondary control system measures the temperature difference between the two containers and adjusts the difference to zero by controlling the differential component of the heating power (O'Neill 1966). This differential power is recorded and appears on the *y* axis of DSC scans. Each point along the DSC scan is proportional to the instantaneous specific heat of the sample. By employing a standard of known heat capacity (*e.g.*, sapphire), it is possible to obtain accurate data on heat capacity for an unknown sample. In this case, we considered it unnecessary to use a standard for a comparative study as experimental conditions were identical for all samples, and as the heat capacity of stoichiometric bornite over a range of temperatures has been adequately determined by Robie *et al.* (1994).

DSC analysis was performed using a Perkin–Elmer DSC 7 differential scanning calorimeter. Each sample chip was weighed to a precision of 0.002 mg and placed in an Al sample tray, which was in turn inserted into the lidded Pt sample container of the calorimeter. An empty Al tray of precisely the same weight as the sample tray was inserted into the calorimeter's reference container. The sample environment in the calorimeter was purged with a constant flow of dry N_2 gas at 2 atmospheres pressure. Each DSC analytical cycle consisted of a heating scan at 10°C/minute from 50° to 300°C followed by a cooling scan at 5°C/minute from 300° to 50°C. Before each analytical run, the scan baseline was obtained by running empty sample pans and corrected for both curvature and slope. Transition temperature and transition-energy calibration were performed using the onset and area of endothermic melting peaks of ultrapure In (156.60°C; 28.45 $J.g^{-1}$) and Sn (231.88°C; 60.46 $J.g^{-1}$), following the two-point calibration routine described by Callanan & Sullivan (1986). Weighing of the sample chips after analysis showed that no measurable loss in mass had occurred over the course of the scans, indicating that sample stoichiometry had not been modified by S loss. Energies of transitions were determined using the same peak-area measurement routines used for the calibration of the instrument. We estimate the systematic error for temperature measurements to have been in the region of ±1–2°C or better.

Electron-Microprobe Analysis

Electron-microprobe analysis of the bornite samples was performed on polished mounts of the bornite samples using a Cameca SX–50 probe at the University of Cambridge, operating in wavelength-dispersion mode. Chalcocite (Cu_2S) was used as a standard for Cu, and pyrite (FeS_2) for Fe and S, and the beam current and accelerating voltage were 50 nA and 20 kV, respectively. Both samples and standards were repolished and stored under vacuum before carbon-coating to inhibit the formation of a surface tarnish. At least 10 analyses were performed on each sample in order to check compositional homogeneity. Some systematic error in the measurement of the exact chemical composition of bornite using electron-microprobe data was anticipated, as several factors, such as migration of cations (Grace & Putnis 1976, Losch & Monhemius 1976) and small losses of S from the volume of excitation under typical analytical conditions, have never been quantified. We found that metal migration and S loss were essentially eliminated by using a defocused beam, giving a spot 20 μm in diameter, with which no change in composition could be detected on increasing counting time. This contrasts with the use of the standard 1 μm spot, where Cu:Fe and *Me*:S ratios do vary appreciably with increased exposure to the electron beam. Previous probe analyses of synthetic copper–iron sulfide standards conducted using the 20 μm spot have shown excellent agreement with the quantities of Cu, Fe and S measured during synthesis, such that the accuracy of the technique was considered satisfactory for the purposes of this study.

Bornite Compositions: Results and Discussion

Details of bornite samples used in this study and compositional data obtained from electron-microprobe analyses are given in Table 1. As can be seen in Figure 2, there is comparatively little compositional variation among samples from the various ore-deposit types and synthetic phases possessing the bornite structure,

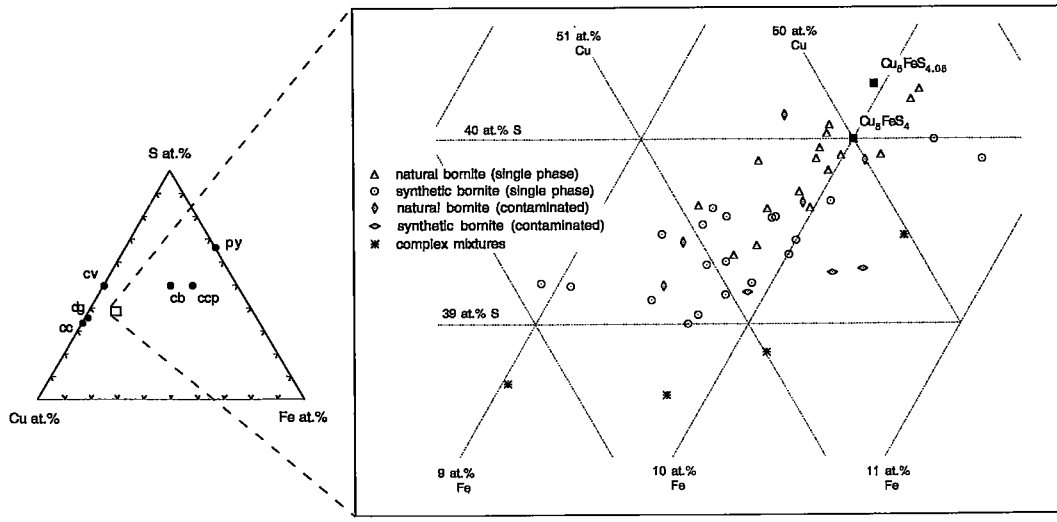

FIG. 2. Compositions of bornite used in this study (right) shown in Cu–Fe–S space, with ideal formulas for bornite and "x-bornite" superimposed as filled squares. Compositions of other common phases in the Cu–Fe–S system are shown for comparison (left). Symbols for the phases are as follows: cc chalcocite, dg digenite, cv covellite, cb cubanite, ccp chalcopyrite, and py pyrite.

all being defined within 1–2 atomic % of the ideal stoichiometric Cu, Fe and S contents. The natural bornite samples show some degree of clustering around Cu_5FeS_4, whereas most samples of synthetic bornite are of compositions somewhat richer in Cu and poorer in S than this. A marked feature of the overall distribution is the narrow compositional band defined by bornite having an Fe content between 9.4 and 10.2 atomic %. Most of the samples of synthetic bornite in this band were not deliberately synthesized with this bulk composition, but have modified their composition either by exsolving other Cu-sulfide phases or condensing elemental sulfur in the synthesis tubes on cooling. Four of the synthetic samples that are S-deficient (ttb26, 27, 38, 39) were found by X-ray diffraction to consist of a complex mixture of phases rather than bornite (Fig. 2), and were therefore excluded from further consideration. In the course of our investigations, we also noted that some other samples, though predominantly low bornite, are contaminated with other Cu–S phases (Table 1). In most cases, these contaminants are microscopically visible, as chalcocite, djurleite or digenite present as small blebs or microveinlets in the case of natural samples, and typically as thin grain-boundary segregations in synthetic bornite. These contaminants, unless in trace amounts, had deleterious effects on our DSC measurements. This theme will be discussed further in the section on DSC results. Electron-microprobe analyses of these samples were performed on parts of the specimen where overlap with the contaminating phase could be avoided, thus the compositions pertain to the bornite component of the samples.

The comparatively small degree of compositional variation shown by single-phase bornite in this study would seem to indicate that the subsolvus free energy – composition curve for low bornite is extremely narrow, despite the large degree of solid solution exhibited with digenite at temperatures above approximately 350°C (Morimoto & Kullerud 1966) and with chalcopyrite above 600°C (Durazzo & Taylor 1982). That no natural samples show deviation from Cu_5FeS_4 by more than 1 at.% in any elemental component (Fig. 2) seems to suggest that the thermodynamic driving force toward stoichiometry during crystallization and cooling is relatively strong, consistent with this hypothesis. The slightly higher degree of deviation from stoichiometry in synthetic samples is probably related to the fact that dry synthesis, which relies on solid-state reactions in a closed system, allows some degree of compositional modification of the end product, but is not a good analogue of processes of ore deposition, which typically involve precipitation from aqueous solution. The latter process would more likely result in deposition of bornite of compositions closer to the free energy minimum owing to possibility of solution – mineral interaction and chemical exchange, which are accelerated in the presence of a fluid phase.

We were unable to synthesize single-phase bornite with compositions containing more sulfur than that expected of stoichiometric bornite, hence the aforementioned distribution in Figure 2. Attempts to

synthesize S-rich bornite in this and earlier studies (Brett & Yund 1964, Yund & Kullerud 1966, Durazzo & Taylor 1982) by decreasing the *Me*:S ratio appreciably from 1.5 typically lead, on quenching, to the separation of digenite, chalcopyrite, or both depending on the ratio Cu:Fe. This behavior seems to result from a combination of the apparent thermodynamic stability of stoichiometric bornite mentioned above, and the rapid kinetics of exsolution along both the bornite–digenite and bornite–chalcopyrite joins. Such rapid kinetics are facilitated by the high population of vacancies in the metal site in compositions near bornite, which allows for rapid diffusion of cations. Berger & Bucur (1996) have shown in potentiometric experiments that at room temperature, the rates of Cu diffusion in bornite approach those of fast-ion conductors, accounting for the fact that even rapid quenching of bornite–chalcopyrite solid solutions can result in the exsolution of optically visible lamellae of chalcopyrite (Durazzo & Taylor 1982). Furthermore, the bornite, chalcopyrite and digenite structures are all based on the same cubic close-packed framework of sulfur atoms, reducing the structural reorganization necessary for exsolution to the diffusion of the interstitial cations and re-ordering of vacancies.

Single-phase S-rich bornite is known, however, and examples from Utah and New Mexico were described by Brett & Yund (1964), and from Alaska and Cornwall by Yund & Kullerud (1966). Such so-called anomalous or "x-bornite" occurs in red-bed-type Cu deposits, roll-front U deposits, and in zones of supergene enrichment, and is generally believed to have been deposited at temperatures below 75°C (Brett & Yund 1964). Brett & Yund provided no chemical analyses of the S-rich bornite they examined, but cell parameters measured before heating suggest compositions of approximately $Cu_5FeS_{4.05}$. Yund & Kullerud (1966) were able to identify x-bornite together with other exsolved products in samples synthesized with S contents of greater that 25.75 wt.%, but were not able to fully characterize this phase. That natural S-rich bornite is not stable at higher temperatures is demonstrated by the fact that it decomposes within minutes into mixtures of stoichiometric bornite, digenite and chalcopyrite on heating above 150°C (Brett & Yund 1964). We noted no bornite in our sample set with a S-content greater than 25.76 wt.%. The sample showing this highest S-content comes from a mesothermal deposit (ttb05). According to the phase diagram of Yund & Kullerud (1966), this composition falls into the field of bornite + x-bornite below 105°C. No second phase was evident from X-ray, optical, and calorimetric characterization of this sample, however, suggesting that exsolution of S-rich bornite or other phases did not occur over the time-scale of our thermal experiments.

The compositional band described above is worthy of some consideration, especially since it does not lie on the bornite–digenite join, but is comprised of samples of apparently single-phase bornite somewhat richer in Fe than bulk compositions along this join. The implication is that the presence of this slight excess of Fe stabilizes Cu-rich bornite relative to the assemblage stoichiometric bornite + digenite. That the band also includes several samples of Cu-rich bornite from mesothermal deposits, which have probably been subject to natural subsolvus annealing and equilibration for periods considerably in excess of typical laboratory time-scales, provides an argument against metastability in this case.

Our investigations of the compositional variation of bornite within our sample set have emphasized the need for care in the use of the electron microprobe to analyze ore minerals that have vacancy-rich structures and low activation energies for the diffusion of component metals. The large deviations in bornite compositions reported in the literature must be viewed with caution if the method of analysis involves a high-intensity, small-diameter electron beam. Where possible, a large-diameter spot should be employed, and extended counting times avoided. Furthermore, samples should be scrutinized for the presence of the extremely common exsolution-derived micro-inclusions, which can result in spurious bulk-compositions, using other analytical methods such as X-ray diffraction and microscopy.

Thermal Analysis: Results and Discussion

Results of the DSC measurements performed in this study are given in Table 2. DSC scans of all the bornite samples analyzed show the two distinct endothermic peaks noted by earlier investigators (Kanazawa *et al.* 1978, Robie *et al.* 1994) at approximately 200° and 260°C (Figs. 1, 3), corresponding to the low–intermediate and intermediate–high phase transitions, respectively. The thermal anomaly associated with the low–intermediate transition is typically the sharper and narrower of the two, with both of these characteristics increasing in the cooling scans. The region of the scan between these two peaks represents the temperature range over which intermediate $2a$-bornite exists (Fig. 1), as verified by the *in situ* neutron-diffraction study of Grguric *et al.* (1996). This region is characteristically raised above the baseline, and slightly inclined in the direction of high temperature, consistent with a process of gradual disordering. The range of temperatures over which the thermal peaks of synthetic samples occurs is considerably wider, corresponding to the wider degree of compositional variation. Peaks of thermal anomalies associated with the low–intermediate transition during the heating scan vary between 197 and 207°C in natural bornite and 154 and 201°C in synthetic bornite (Table 2). The intermediate–high transition peaks occurred between 259 and 273°C in natural samples and 239 and 271°C in synthetic samples.

TABLE 2. PHASE TRANSITIONS IN BORNITE: DIFFERENTIAL SCANNING CALORIMETRY DATA

	HEATING SCAN				COOLING SCAN				HYSTERESIS	
Sample	Peak (°C) low-int.	Peak (°C) int.-high	ΔH (J.g) low-int.	ΔH (J/g) int.-high	Peak (°C) low-int.	Peak (°C) int.-high	ΔH (J/g) low-int.	ΔH (J/g) int.-high	low-int. (°C)	int.-high (°C)
ttb01	202.4	265.5	8.41	1.88	164.1	261.4	-5.93	-1.58	38.3	4.1
ttb02	197.0	264.0	7.09	1.60	150.9	253.3	-5.91	-1.79	46.0	10.7
ttb03	204.2	267.4	8.59	1.16	165.3	263.4	-5.58	-1.86	39.0	4.0
ttb04	207.2	265.9	9.80	1.76	168.8	263.3	-6.26	-2.08	38.5	2.6
ttb05	207.4	266.0	8.35	1.15	168.4	263.4	-5.32	-1.81	39.0	2.7
ttb06	205.8	261.9	7.95	1.00	169.0	259.5	-4.73	-0.58	36.8	2.5
ttb07	208.5	266.1	10.01	1.63	168.4	263.8	-6.37	-2.25	38.1	2.4
ttb08	207.4	265.8	9.78	1.28	168.4	263.0	-6.31	-2.04	39.0	2.8
ttb09	206.1	265.6	7.41	1.30	167.0	263.1	-4.65	-1.61	39.1	2.5
ttb10	204.0	273.5	6.74	1.00	162.8	268.9	-3.43	-1.11	41.2	4.6
ttb11	206.0	265.7	6.55	0.83	168.7	262.7	-4.11	-0.79	36.3	3.1
ttb12	204.7	259.3	6.29	0.99	167.9	254.8	-3.63	-0.02	36.8	4.5
ttb13	206.2	268.6	9.16	1.21	163.8	263.9	-5.75	-1.85	42.3	4.7
ttb14	207.0	266.7	9.62	1.33	168.0	263.0	-6.04	-2.03	39.0	3.6
ttb15	204.8	265.2	8.76	1.35	-	-	-	-	-	-
ttb16	205.9	265.8	9.91	1.29	168.1	262.7	-6.30	-1.97	37.7	3.1
ttb17	196.5	264.3	5.82	0.80	150.8	254.0	-4.64	-0.64	45.7	10.3
ttb18	204.5	265.6	8.45	0.83	167.9	263.5	-0.57	-0.81	36.6	2.1
ttb19	204.9	266.8	9.57	1.31	168.1	264.0	-6.15	-2.11	36.8	2.8
ttb20	207.1	265.7	8.24	1.25	167.4	262.8	-5.03	-1.49	39.7	2.8
ttb21	209.0	266.8	10.20	2.05	169.1	263.8	-6.45	-1.97	39.8	3.0
ttb22	201.5	266.6	6.93	1.38	166.4	262.4	-5.65	-2.00	35.1	4.2
ttb23	199.4	265.8	5.71	1.47	166.0	262.4	-5.56	-1.96	33.4	3.4
ttb24	178.4	259.9	2.80	1.06	141.3	257.2	-2.20	-0.74	37.1	2.7
ttb25	172.8	254.9	2.24	1.06	147.0	-	-4.89	-	25.8	-
ttb26	-	-	-	-	-	-	-	-	-	-
ttb27	-	-	-	-	-	-	-	-	-	-
ttb28	185.3	239.3	5.97	0.92	143.7	236.4	-5.46	-1.18	41.6	4.0
ttb29	186.0	239.3	6.88	1.04	145.0	236.8	-5.71	-1.18	41.0	3.5
ttb30	155.4	262.9	0.86	1.42	117.0	260.2	-2.32	-1.11	38.4	2.7
ttb31	154.1	260.8	0.92	1.07	107.7	257.3	-1.84	-0.96	46.4	3.5
ttb32	160.8	244.9	1.51	1.21	104.7	242.7	-1.86	-0.94	56.1	2.2
ttb33	161.4	242.6	1.44	1.12	9.8	240.9	-0.76	-0.99	151.6	1.6
ttb34	198.8	256.4	6.28	1.18	160.0	251.9	-5.55	-1.93	38.7	3.5
ttb35	199.3	256.9	7.27	1.59	-	-	-	-	-	-
ttb36	196.6	270.7	8.80	1.47	167.4	267.1	-6.26	-1.49	29.2	3.6
ttb37	197.1	268.2	6.64	1.29	162.2	264.9	-4.95	-2.01	34.9	3.3
ttb38	-	245.3	-	0.95	89.2	242.5	-0.68	-0.64	-	2.7
ttb39	-	245.1	-	0.70	69.9	241.9	-0.66	-0.64	-	3.2
ttb40	195.2	261.4	5.28	1.43	162.2	258.6	-5.47	-1.88	33.0	2.9
ttb41	189.7	260.2	4.36	1.53	158.1	258.1	-4.84	-1.50	31.6	2.1
ttb42	196.8	262.0	5.44	1.41	162.4	258.4	-5.59	-1.49	34.4	3.6
ttb43	190.6	255.1	3.56	1.51	154.2	252.3	-4.37	-1.62	36.5	2.8
ttb44	197.8	260.7	7.39	1.43	164.6	258.8	-6.14	-1.50	33.3	1.9
ttb45	201.0	262.7	7.94	1.50	164.5	259.2	-6.24	-1.67	36.5	3.5
ttb46	198.1	261.9	6.99	1.14	157.7	258.9	-5.88	-1.82	40.4	3.0
ttb47	197.8	260.7	6.57	1.22	165.1	258.7	-5.76	-1.67	32.8	2.0
ttb48	198.7	256.4	7.33	1.36	163.5	254.5	-6.28	-1.60	35.3	1.9

We found that the presence of contaminating phases in both natural and synthetic samples had a deleterious effect on our DSC results owing to both interference from transition peaks in the contaminating phases and more seriously to diffusive exchange of components between the contaminants and the host bornite. The scan of contaminated sample ttb12 (Fig. 1) shows the distinctive doublet of the chalcocite α–β transition in the heating scan, which is replaced by a single peak corresponding to the high–low digenite transition during the cooling scan. We ascribe this behavior to net diffusion of Cu from the chalcocite impurity into the host bornite. This loss of Cu from the chalcocite, combined with annealing over the timescale of the experiment, resulted in its conversion to digenite. The locally elevated levels of Cu in the host bornite resulted in a second slightly Cu-enriched bornite phase coexisting with the unaffected bornite, accounting for the two weak high–intermediate transition peaks and splitting of the intermediate–low peak (Fig. 1). The rapid kinetics of these diffusion-controlled processes are consistent with the aforementioned findings of Berger & Bucur (1996). Because the effects of these interactions were difficult to quantify, we excluded samples with more than minor amounts of contaminating phases (Table 1) from further consideration.

In the remaining samples, we noted a correlation between the Fe content and Cu:Fe value of bornite on one hand and the peak attributed to the intermediate–high transition. Plots of the temperature of this transition (T_c) against these compositional parameters (Figs. 4a, b) show a band-like distribution of points with an apparently linear relationship. These correlations are more clearly evident for the synthetic samples since they exhibit more compositional variation in all elemental components. A least-squares fit to the data on the synthetic samples gave the following relationships:

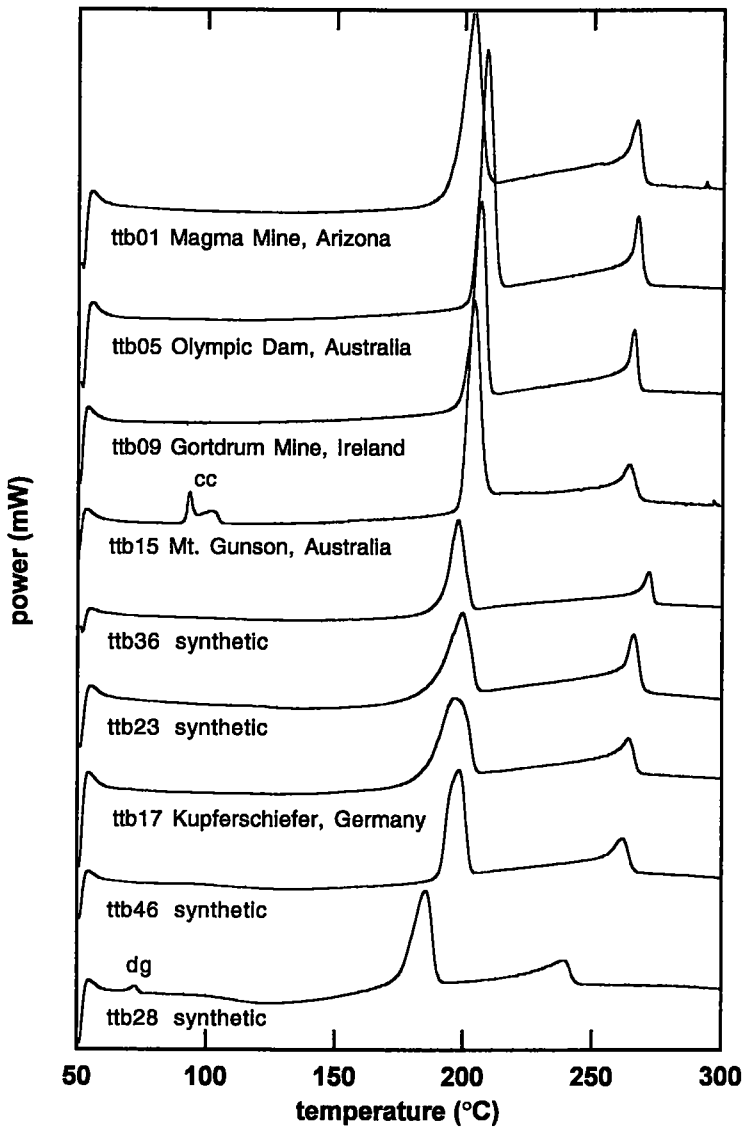

FIG. 3. DSC heating-scan profiles of natural and synthetic samples of bornite illustrating variation in temperatures of endothermic peaks associated with both low–intermediate and intermediate–high transitions. Heating rate was 10°C/minute. Peaks due to impurity phases are labeled: dg digenite, cc chalcocite.

$$T_c^{\text{int-high}}\ (°C) = 18.9 \bullet (\text{Fe content, in atom \%}) + 74 \quad (1)$$

$$T_c^{\text{int-high}}\ (°C) = -27.8 \bullet (\text{Cu:Fe, atomic}) + 403 \quad (2)$$

over the compositional range of our sample set. Calculated standard deviations in m and b parameters were ±2.34 and ±22.9, respectively, for Equation (1) and ±3.55 and ±18.5, respectively, for Equation (2). No such correlations were seen for Cu or S content alone, indicating the importance of the role of Fe in determining the intermediate–high transition temperature. The sensitivity of this behavior is clearly shown in Figure 4a, where variation in Fe content of only 1.5 at. % results a difference in T_c of approximately 35°C.

Intriguingly, however, no correlation was observed between the peak of the low–intermediate transition

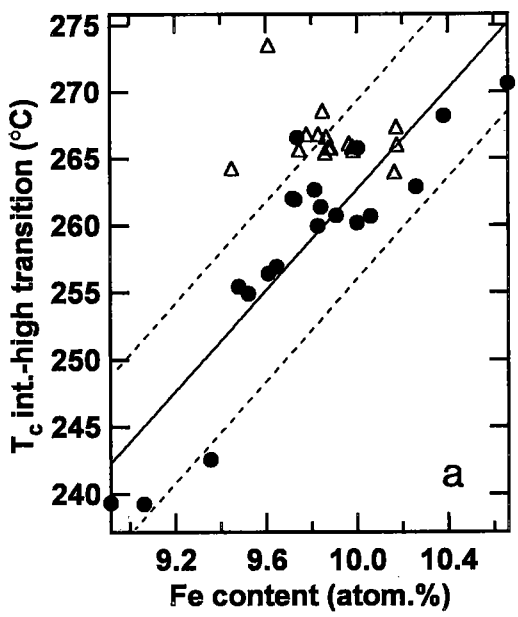

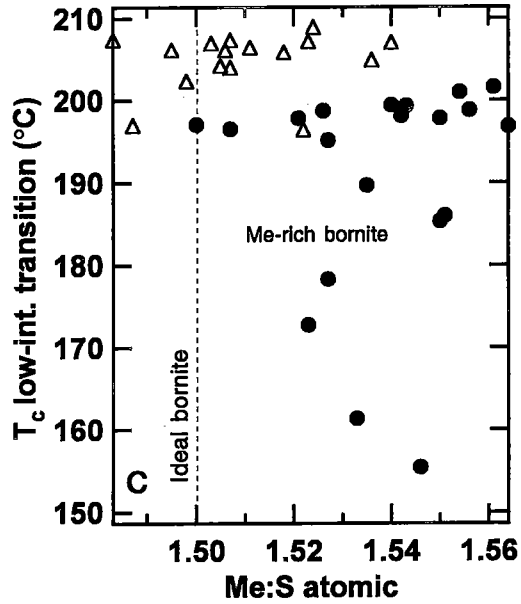

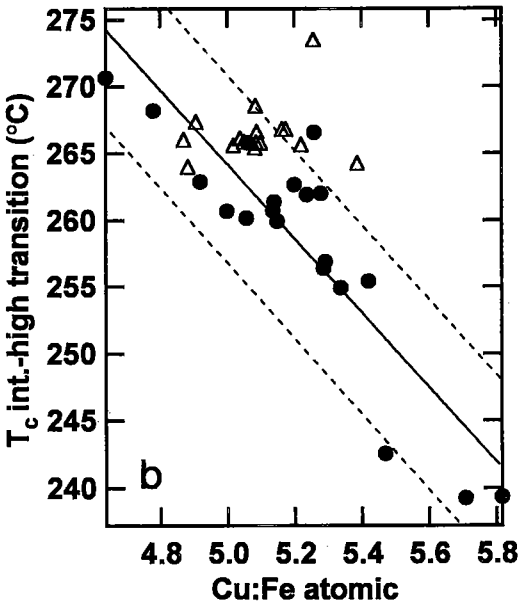

FIG. 4. Temperatures of transitions in bornite plotted against compositional parameters (Fe content in a, Cu:Fe in b, and *Me*:S in c). Synthetic samples are shown as filled circles, and natural samples, as open triangles. Linear fits (solid lines) utilize data from synthetic samples only. Dashed lines are guides for the eye.

and any of the compositional parameters mentioned above. Since this transition has been suggested to involve short-range vacancy-ordering and associated cation-site offsets (Koto & Morimoto 1975, Pierce & Buseck 1978), we anticipated that *Me*:S ratios might strongly influence T_c, because the *Me*:S ratio relates directly to the cation:vacancy ratio of the bornite structure. A plot of *Me*:S against T_c for this transition (Fig. 4c) illustrates the lack of any meaningful correlation between these parameters. This does not rule out the possibility that there is a compositional control on this transition, as the accurate measurement of populations of vacancies is difficult, and the use of the *Me*:S ratio alone may be inadequate. The presence of quenched-in vacancies and trace impurities are likely to influence T_c in addition, the former being more important in synthetic samples, and the latter, in natural samples; their concentrations were not determined in this study. An important observation in Figure 4c is the fact that all the synthetic samples have a lower value of T_c than natural samples of similar *Me*:S ratio. This T_c offset could conceivably result from a contribution from quenched-in vacancies to the population of vacancies and the lower impurity content of the synthetic samples, the latter resulting in weaker pinning of vacancies, thus allowing the transition to initiate at lower temperatures. The fact that those samples doped with trace elements (ttb44–47, Table 1) have a relatively high T_c for the low–intermediate transition lends some credence to this hypothesis.

Implications for Transition Mechanisms

The above-mentioned correlation between major-element compositional parameters and T_c for the intermediate–high transition and the notable lack thereof for the lower-temperature transition seem to suggest that the two transitions are the result of different structural processes. This inference is supported by the fact that the low–intermediate transition is a first-order discontinuous process (hence we have defined T_c for this transition as the peak maximum), with characteristically large thermal hysteresis, whereas the intermediate–high transition is more gradual, with minor thermal hysteresis (Fig. 1, Table 2). The peak of the intermediate–high transition as tabulated here refers to the sharp endothermic peak at approximately 265°C (Fig. 1), which corresponds to the point at which diffraction peaks related to the $2a$ superstructure disappear. On the basis of the intensities of $2a$-supercell reflections measured in neutron-diffraction patterns, however (Grguric *et al.* 1996, 1998), this transition is tricritical, and the disordering process associated with it begins almost immediately up-temperature of the low–intermediate transition. The profile of the thermal anomaly associated with the intermediate–high transition is consistent with the behavior of the specific heat for a tricritical transition, as defined in Salje (1990), allowing for some deviations from ideal tricritical behavior due to critical fluctuations near T_c. The specific heat increases with temperature near T_c in a tricritical transition according to the relationship:

$$\Delta c_p \propto (T_c - T)^{-0.5} \quad (3)$$

We have therefore defined T_c for the intermediate–high transition as the peak of the thermal anomaly. Overall, the tricritical nature of this transition, the sensitivity to cation ratio variation, and the down-temperature development of antiphase domains (Putnis & Grace 1976) are not inconsistent with a cation order–disorder transition, as proposed by Kanazawa *et al.* (1978).

On the basis of the interpretation of our thermal experiments, it follows that the temperature at which the differentiation of Fe and Cu atoms into alternate a subcells is lost is linearly related to the Fe content and Cu:Fe ratio of bornite. Why this transition is particularly sensitive to variation in compositional parameters involving Fe and not sensitive to Cu content independently is unclear, however. The importance of Fe in stabilizing the various types of superstructures observed in the bornite–digenite solid solution is well established, although once again the exact mechanism of this stabilization is unknown. All natural samples of digenite contain approximately 1 at. % Fe, which has been shown by Morimoto & Gyobu (1971) to stabilize the $5a$ superstructure of this phase relative to anilite + djurleite assemblages below 80°C. Attempts by these investigators to stabilize the $5a$ superstructure by substituting chemically similar elements, such as Co and Ni, for Fe failed, indicating the importance of this component. In their TEM studies, Putnis & Grace (1976) and Pierce & Buseck (1978) showed that slight modifications to the Fe content of bornite could be effected by differential heating of the sample with the electron beam. This resulted in the breakdown of the stable $2a4a2a$ superstructure to various other superstructures, none of which are known to occur naturally, a testament to their metastability and, therefore a reinforcement of the importance of Fe in stabilizing this end-member. In demonstrating the existence of a highly sensitive linear relationship between Fe content and the temperature required to induce transitions in bornite, we underscore the importance of Fe in this solid solution, although we are no closer to establishing the mechanism of stabilization. The sensitivity of the structure to variation in Fe content may be related to charge-balance effects associated with the presence of this element in the trivalent state, as determined by Mössbauer spectroscopy (Townsend *et al.* 1977). Since Cu in bornite (and digenite) has been shown to be in a monovalent state (Van der Laan *et al.* 1992), we would expect less effect on the overall charge-balance in the structure and other more complex electronic interactions for the same variation in Cu content.

Our observations on the low–intermediate transition described in the previous section seem consistent with the previously proposed models that this transition results from a process of rapid disordering of vacancies, with associated displacements of metal atoms from irregular to regular tetrahedral coordination (Koto & Morimoto 1975, Pierce & Buseck 1978). These combined effects result in an overall increase in symmetry from orthorhombic $2a4a2a$ (pseudotetragonal; Koto & Morimoto 1975) to cubic $2a$. The fact that this transition can occur at room temperature after several days (Morimoto & Kullerud 1961) suggests that an extensive long-range diffusion process is not involved. This proposal is consistent with the model of Pierce and Buseck for the transition, which involves short-range ordering of vacancies within the zinc-blende-structured subcells. Vacancy clustering into these cells occurs simultaneously with the cation-ordering process during the high–intermediate transition (Kanazawa *et al.* 1978). It would seem that if both short-range vacancy ordering and resultant metal offsets in tetrahedral sites are involved, the former process would be the rate-controlling step for the transition, since the latter would be essentially instantaneous (phonon frequency). As postulated, this vacancy-ordering mechanism could mean that the low–intermediate transition in bornite is sensitive to a host of factors and interactions relating to the population of vacancies and their diffusion behavior.

CONCLUSIONS

1. Natural samples of bornite that deviate significantly from stoichiometry are rare, a consequence of the thermodynamic stability of stoichiometric bornite and the rapidity of exsolution at geologically low temperatures. Our characterization of natural and synthetic bornite compositions seems to suggest, however, that the stability field of single-phase bornite may include compositions that are slightly poorer in Fe and S and richer in Cu than Cu_5FeS_4, extending out to $Cu_{5.15}Fe_{0.95}S_{3.9}$.

2. The peaks of thermal anomalies coincident with the intermediate–high transition in bornite are linearly related to the atomic Fe content and Cu:Fe ratios over the compositional range of our sample set. Similar relationships are observed during the cooling cycle of the scans, but refer to the onset of the short-range ordering transition rather than the polymorphic high–intermediate transition measured by neutron powder diffraction. This is a consequence of the formation of antiphase domains (Grguric *et al.* 1998, Putnis & Grace 1976).

3. In contrast, the lack of any meaningful correlation between the transition temperature of the low–intermediate transition and any compositional parameter determined here seems to suggest a fundamental difference in the mechanism of this transition. The short-range vacancy ordering and cation off-centering mechanisms proposed by previous investigators could conceivably be influenced by a number of factors and interactions relating to the population of vacancies and their diffusion behavior. In addition to the metal: sulfur ratio, these factors could include thermal history, trace-element concentrations, and dislocation density in the samples.

ACKNOWLEDGEMENTS

The authors thank Dr. Richard Harrison for assistance with DSC analysis and for helpful discussions. We are also grateful for the assistance of Brian Cullum with sample synthesis and Dr. Stephen Reed with electron-microprobe analysis. Specimens from the Olympic Dam mine were kindly donated by WMC Resources Ltd. We thank Dr. Graham Chinner for permission to use samples from the Cambridge Mineral Collection. The helpful comments and suggestions made by the reviewers of the manuscript were appreciated.

REFERENCES

BERGER, R. & BUCUR, R.V. (1996): Potentiometric measurements of copper diffusion in polycrystalline chalcocite, chalcopyrite and bornite. *Solid State Ionics* **89**, 269-278.

BRETT, R. & YUND, R.A. (1964): Sulfur-rich bornites. *Am. Mineral.* **49**, 1084-1098.

CALLANAN, J.E. & SULLIVAN, S.A. (1986): Development of standard operating procedures for differential scanning calorimeters. *Rev. Sci. Instrum.* **57**, 2584-2592.

DURAZZO, A. & TAYLOR, L.A. (1982): Experimental exsolution textures in the system bornite–chalcopyrite: genetic implications concerning natural ores. *Mineral. Deposita* **17**, 79-97.

FRUEH, A.J. (1950): Disorder in the mineral bornite, Cu_5FeS_4. *Am. Mineral.* **35**, 185-192.

GRACE, J. & PUTNIS, A. (1976): Thermal decomposition and cation mobility in bornite. *Econ. Geol.* **71**, 1058-1059.

GRGURIC, B.A., DOVE, M.T., HARRISON, R.J. & PUTNIS, A. (1996): A neutron diffraction study of phase transitions and superstructures in bornite Cu_5FeS_4. *Terra Nova Abstr., Suppl.* **1, 8**, 25.

_____, PUTNIS, A. & HARRISON, R.J. (1998): An investigation of the phase transitions in bornite (Cu_5FeS_4) using neutron diffraction and differential scanning calorimetry. *Am. Mineral.* **83** (in press).

KANAZAWA, Y., KOTO, K. & MORIMOTO, N. (1978): Bornite (Cu_5FeS_4): stability and crystal structure of the intermediate form. *Can. Mineral.* **16**, 397-404.

KOTO, K. & MORIMOTO, N. (1975): Superstructure investigation of bornite Cu_5FeS_4, by the modified partial Patterson function. *Acta Crystallogr.* **B31**, 2268-2273.

LOSCH, W. & MONHEMIUS, A.J. (1976): An AES study of a copper–iron sulfide mineral. *Surface Sci.* **60**, 196-210.

MORIMOTO, N. (1964): Structures of two polymorphic forms of Cu_5FeS_4. *Acta Crystallogr.* **17**, 351-360.

_____ & GYOBU, A. (1971): The composition and stability of digenite. *Am. Mineral.* **56**, 1889-1909.

_____ & KULLERUD, G. (1961): Polymorphism in bornite. *Am. Mineral.* **46**, 1270-1282.

_____ & _____ (1966): Polymorphism on the Cu_9S_5 – Cu_5FeS_4 join. *Z. Kristallogr.* **123**, 235-254.

O'NEILL, M.J. (1966): Measurement of specific heat functions by differential scanning calorimetry. *Anal. Chem.* **38**, 1331-1336.

PANKRATZ, L.B. & KING, E.G. (1970): High-temperature enthalpies and entropies of chalcopyrite and bornite. *U.S. Bur. Mines, Rep. Invest.* **7435**.

PIERCE, L. & BUSECK, P.R. (1978): Superstructuring in the bornite–digenite series: a high resolution electron microscopy study. *Am. Mineral.* **63**, 1-16.

PUTNIS, A. & GRACE, J. (1976): The transformation behaviour of bornite. *Contrib. Mineral. Petrol.* **55**, 311-315.

ROBIE, R.A., SEAL, R.R., II & HEMINGWAY, B.S. (1994): Heat capacity and entropy of bornite (Cu_5FeS_4) between 6 and 760 K and the thermodynamic properties of phases in the system Cu–Fe–S. *Can. Mineral.* **32**, 945-956.

SALJE, E.K.H. (1990): *Phase Transitions in Ferroelastic and Co-elastic Crystals*. Cambridge University Press, Cambridge, U.K.

TOWNSEND, M.G., GOSSELIN, J.R., TREMBLAY, R.J., RIPLEY, L.G., CARSON, D.W. & MUIR, W.B. (1977): A magnetic and Mössbauer study of magnetic ordering and vacancy clustering in Cu_5FeS_4. *J. Phys. Chem. Solids* **38**, 1153-1159.

VAN DER LAAN, G., PATTRICK, R.A.D., HENDERSON, C.M.B. & VAUGHAN, D.J. (1992): Oxidation state variations in copper minerals studied with Cu 2*p* X-ray absorption spectroscopy. *J. Phys. Chem. Solids* **53**, 1185-1190.

YUND, R.A. & KULLERUD, G. (1966): Thermal stability of assemblages in the Cu–Fe–S system. *J. Petrol.* **7**, 454-488.

Received July 14, 1997, revised manuscript accepted January 23, 1998.